

Additive manufacturing of multifunctional polylactic acid (PLA)—multiwalled carbon nanotubes (MWCNTs) nanocomposites

Nectarios Vidakis, Markos Petousis, Mirto Kourinou, Emmanuel Velidakis, Nikolaos Mountakis, Peder Erik Fischer-Griffiths, Sotirios Grammatikos & Lazaros Tzounis

To cite this article: Nectarios Vidakis, Markos Petousis, Mirto Kourinou, Emmanuel Velidakis, Nikolaos Mountakis, Peder Erik Fischer-Griffiths, Sotirios Grammatikos & Lazaros Tzounis (2021) Additive manufacturing of multifunctional polylactic acid (PLA)—multiwalled carbon nanotubes (MWCNTs) nanocomposites, *Nanocomposites*, 7:1, 184-199, DOI: [10.1080/20550324.2021.2000231](https://doi.org/10.1080/20550324.2021.2000231)

To link to this article: <https://doi.org/10.1080/20550324.2021.2000231>



© 2021 The Author(s). Published by Informa UK Limited, trading as Taylor & Francis Group.



Published online: 12 Nov 2021.



[Submit your article to this journal](#)



Article views: 1683



[View related articles](#)




[View Crossmark data](#)



Citing articles: 1 [View citing articles](#)

Additive manufacturing of multifunctional polylactic acid (PLA)—multiwalled carbon nanotubes (MWCNTs) nanocomposites

Nectarios Vidakis^a, Markos Petousis^a , Mirto Kourinou^a, Emmanuel Velidakis^a, Nikolaos Mountakis^a, Peder Erik Fischer-Griffiths^b, Sotirios Grammatikos^b and Lazaros Tzounis^a

^aMechanical Engineering Department, Hellenic Mediterranean University, Heraklion, Crete, Greece; ^bGroup of Sustainable Composites, Department of Manufacturing and Civil Engineering, Norwegian University of Science and Technology, Gjøvik, Norway

ABSTRACT

In this work, an industrially scalable method was developed for the preparation of multifunctional nanocomposite filaments. Polylactic Acid (PLA) polymer matrix was enriched with Multi Wall Carbon Nanotubes (MWCNT) at various concentrations, to fabricate 3D-printed parts by the Fused Filament Fabrication (FFF) technology. The effect of the nanofiller loading at the mechanical, thermal, electrical, thermomechanical, and antibacterial performance of the novel nanocomposites fabricated in this work was investigated. The filler loading of 5 wt.% was also tested to reveal its electrothermal Joule heating performance. The antibacterial properties of the nanocomposites were examined through a screening process, against *Escherichia coli* (*E. coli*) and *Staphylococcus aureus* (*S. aureus*). For loadings of 1 wt.% and higher the mechanical properties were significantly improved. The 5 wt.% loading showed measurable antibacterial performance. The nanocomposites prepared herein can be characterized as multifunctional materials, suitable for various industrial applications, such as sensors fabrication, health monitoring devices, etc.

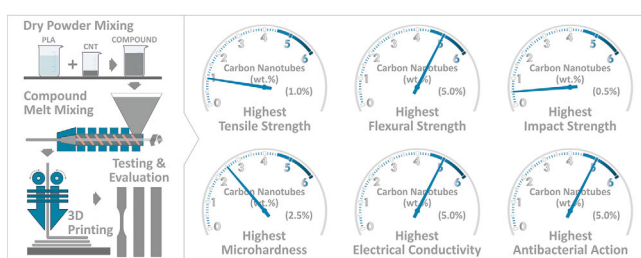
ARTICLE HISTORY

Received 3 August 2021
Accepted 26 October 2021

KEYWORDS

3D printing; conductive polymer composites; nanocomposites; multi-walled carbon nanotubes; polylactic acid; 3D printed electronics; additive manufacturing; fused filament fabrication (FFF)

GRAPHICAL ABSTRACT





1. Introduction

Nanomaterials have at least one dimension in the nanometre scale and nanocomposites are mixtures between a matrix material and nanofillers [1]. The result of the nanoparticles' addition to the matrix, often leads to improvement in its inherent properties; namely the strength and stiffness, electrical conductivity, thermal conductivity and/or thermal stability, chemical resistance, gas separation, etc., amongst others [2,3]. Conductive nanofillers for example can be used to transform an insulating polymer matrix into a conductive material, as it has been several times reported to date [4–6].

Carbon nanotubes (CNTs) are used as fillers to improve properties of the resulting polymer

nanocomposites [7], such as the electrical conductivity and the Young's modulus; both of them known to be achieved above a critical CNT volume fraction, which is defined and often reported as percolation threshold [8]. Polymers are widely used as matrix in nano- and micro-scale reinforced composite materials, due to their low cost, light-weight nature and ease of processability [1,9]. Polylactic Acid (PLA) is a linear, aliphatic polyester synthesized from lactic acid, which can be produced from renewable resources [10–14]. It's a biodegradable thermoplastic polyester [15] and one of the most promising polymers because of its unique physical properties that make it ideal for countless applications [16–21], making it also very popular in 3D printing [22].

CONTACT Markos Petousis  markospetousis@hmu.gr  Mechanical Engineering Department, Hellenic Mediterranean University, Estavromenos, Heraklion, Crete, Greece

© 2021 The Author(s). Published by Informa UK Limited, trading as Taylor & Francis Group.

This is an Open Access article distributed under the terms of the Creative Commons Attribution License (<http://creativecommons.org/licenses/by/4.0/>), which permits unrestricted use, distribution, and reproduction in any medium, provided the original work is properly cited.

Three-dimensional printing belongs to the Additive Manufacturing (AM) technologies family [23,24] and is one of the most widely used AM processes in medicine, packaging and printing, due to being a low cost, rapid and facile process [25]. Extrusion-based AM, also known as Fused Filament Fabrication (FFF) [26,27] create structures by extruding material initially in filament form, from a nozzle and depositing it onto the 3D printing platform. The interest for FFF 3D printing is growing, due to the wide range of applications that can be used [28–30].

Novel materials with antimicrobial properties have a vital role in treating infectious diseases that are caused by bacteria and viruses [31–33]. Biomaterials with antibacterial properties are the construction materials for medical devices with the ability to inhibit the growth or kill the pathogenic microorganisms. Polymer materials have shown potential as antibacterial and antiviral agents [34,35]. PLA is a thermoplastic polymer well-known for its biocompatibility and biodegradability properties, while it is one of the most widely used materials nowadays for FFF 3D printing applications [30].

Conductive polymer composites (CPCs) have recently attracted a significant interest in 3D printing Additive Manufacturing (AM) processes. Carbon nanoallotropes introduced in a polymer matrix can convert its inherently insulating nature into a conductive one, yielding lightweight and flexible conductors with variable electrical properties that can be typically tuned by (i) the nanoparticle filler loading, (ii) the particle aspect ratio, (iii) the surface area and surface chemistry, as well as (iv) the processing/mixing parameters that could significantly affect the micro- and nano-dispersion quality. CPCs are known for their sensing functionalities, i.e. (i) gas or liquid chemical and/or electrochemical sensors, (ii) strain sensors for wearables or touch/pressure sensors *via* a piezoresistive or a piezoelectric underlying mechanism, (iii) temperature sensors, etc. [36]. Polymeric filaments with carbon nanoadditives have been fabricated both for mechanical properties enhancement [37] of the resulting FFF 3D printed parts, as well as utilizing the electrically conductive properties of the fillers towards biomedical sensors [38], piezoresistive strain sensors [39], actuators [40], and resistors for Joule-heating [41].

Patanwala et al. [37] reported on 3D printed PLA/CNT nanocomposites focusing only on the mechanical properties of the 3D printed constructs. Relatively, the inclusion of CNTs increased the Young's modulus by 30% at 5% CNT loading but reduced the tensile strength and overall toughness of the FFF parts. Recently, Yang et al. [42] reported

on the preparation of PLA/CNT nanocomposites for FFF application, pointing out that the CNT content has a significant influence on the mechanical properties and conductivity properties. Namely, the addition of 6 wt.% CNT resulted into a 64.12% increase in the tensile and a 29.29% increase in the flexural strength, respectively. The electrical resistivity varied from approximately $1 \times 10^{12} \Omega/\text{sq}$ to $1 \times 10^2 \Omega/\text{sq}$ for CNT contents ranging from 0 wt.% to 8 wt.%, while lower filling velocity, higher liquefier temperature and greater layer thickness were found to be the optimum 3D printing process parameters to obtain 3D printed constructs with the highest electrical conductivity properties. In another work, Mora et al. [43] developed a micromechanics model to determine the electrical conductivity of melt blended PLA/CNT and HDPE/CNT 3D printed nanocomposites, being in good agreement and corroborating experimental results in the same study. Namely, the electrical conductivity of 3D printed PLA/CNT and HDPE/CNT composites was measured for various CNT loadings, while low percolation thresholds were obtained i.e. 0.23 vol. % and 0.18 vol. % of CNTs for PLA/CNT and HDPE/CNT nanocomposites with the highest conductivity values reaching $\sim 1.0 \text{ S/m}$ at filler loading higher than 1.0 vol.% fraction.

PLA/carbon black (CB) CPC filaments for FFF 3D printing and electrically conductive 3D objects have been reported also by Vidakis et al., focusing on the electrical, electrothermal, mechanical and antibacterial properties of the 3D printed nanocomposites [44]. Namely, the electrical percolation threshold was studied, with the nanocomposites exhibiting an electrically conductive behavior already from 2.5 wt.% loading. An anisotropic behavior was reported for the 'through' thickness and 'cross-layer' 3D printing specimens' measurement directions with the highest electrical conductivity (σ) at the 'cross-layer' direction for the PLA/CB (5.0 wt.%) nanocomposite ($\sim 1.0 \text{ S/m}$). Finally, the highest reinforcement especially in tensile and flexural tests was observed for the PLA/CB nanocomposites with 0.5 wt.% filler loading ($\sim 17.1\%$ increase for the tensile strength and $\sim 14.1\%$ increase for the tensile modulus).

Gnanasekaran et al. reported on 3D printing of CNT- and graphene-based CPCs based on a polybutylene terephthalate (PBT)/PLA blends, while they have reported the highest electrical conductivity of 10.0–12.0 S/m for the CNT (at 0.35% vol. fraction) and 1.0–4.0 S/m for the graphene (at 0.85% vol. fraction) nanocomposites, respectively [45]. Also, the authors pointed out that at least $\sim 0.49 \text{ wt.}\%$ of CNT ($\varphi_c \sim 0.31 \text{ vol.}\%$) and $\sim 5.2 \text{ wt.}\%$ ($\varphi_c \sim 3.3 \text{ vol.}\%$) of graphene are required for the FFF

fabrication of CNT- and Graphene-based conductive filaments. Aumtate et al. reported on reinforcing polypropylene (PP) with reduced graphene oxide (rGO)- polylactic acid microcapsules for FFF 3D printed objects. At very low graphene loading (0.75 wt.%), the 3D printed construct showed neither shrinkage nor warping, while the Young's Modulus (E) of the 3D printed graphene nanocomposites increased from 220 MPa (neat PP matrix) to 450 MPa (>100% increase) [46]. In another study related to isotactic polypropylene/graphene 3D printed nanocomposites, the presence of graphene induced shear thinning during extrusion (improved processability aspect), while at 5% and 10% of graphene loading, the storage modulus decreased considerably; namely nearly 50% for the 10% loading [47].

PLA/CNT conductive nanocomposite could be ideal feedstock material for FFF 3D printing processes, and therefore systematic investigations are required to highlight the fundamental process-structure-property relationship. Moreover, the advantage for using MWCNTs in PLA is that CNTs as one-dimensional (1D) nanofillers can easily create networks in the polymer matrix allowing for the charge carrier transport and realising thus a relatively high conductivity at generally low filler loadings. To the best of the author's knowledge, a detailed study of PLA/CNT conductive nanocomposites focusing on (i) the electrical percolation threshold as a function of the filler loading, (ii) the effect of filler loading on the 3D printed constructs' electrical conductivity with respects to the interlayer fusion, as well as (iii) thorough static mechanical and thermomechanical analyses of the 3D printed samples has not been reported yet.

In this study, PLA was mixed with Multi-Walled Carbon Nanotubes (MWCNTs) at various concentrations, to produce 3D printing PLA/MWCNTs nanocomposite filaments using a thermomechanical melt mixing method. This method is employed because of its versatility, the relatively low-cost of the production facilities, the compatibility with industrial processes and its low environmental impact i.e. nanofillers are mixed with the polymer matrix in the melt state without any use of organic solvents as for the solvent-mixing nanocomposites' fabrication [30]. The produced filaments were 3D printed with the FFF process. Specimens were prepared, and then tested for their mechanical, thermal, electrical, electrothermal and antibacterial performance, to fully characterize the novel 3D printed nanocomposites of this work. The nanocomposites' performance was improved as revealed by the analytical techniques carried out, compared to the pure PLA material, especially for filler loadings from

1.0 wt.% and above. PLA/MWCNT nanocomposites prepared herein can be considered as multifunctional materials, that can easily be industrialized for various types of demanding applications, requiring enhanced performance in various fields.

2. Materials and methods

2.1. Materials

Polylactic Acid used as the matrix material in this work was industrial grade PLA (PLA 3052D) in fine powder form procured from Plastika Kritis S.A. (Heraklion, Crete, Greece). According to the supplier's technical specification the polymer's molecular weight was 116,000 g/mol, its Melt Flow Index 14 g/10 min (ASTM D1238), its Tensile Strength at Yield 62 MPa (ASTM D638), its Melting Temperature 153 °C (ASTM D 3418), and its Glass Transition Temperature 57.5 °C (ASTM E1356). MWCNTs (NC 7000) were received from Nanocyl S.A. (Sambreville, Belgium). According to the supplier technical data sheet, MWCNTs (NC7000) is a highly conductive grade material with purity higher than 90%, while the nanotubes exhibit average diameters of 9.5 nm, average lengths of 1.5 μm , density, $\rho \square 2.1 \text{ g/cm}^3$, surface area 250–300 m^2/g and volume resistivity $10^{-4} \Omega \text{ cm}$.

2.2. Methods

The methodology followed in this study for the development and characterization of the PLA/MWCNT nanocomposites is shown in [Figure 1](#).

PLA/MWCNT nanocomposites at 0.1, 0.5, 1.0, 2.5 and 5.0 wt.% were prepared. Initially, the powders were mixed *via* a mechanical mixing process. Then, to eliminate moisture adsorbed by the constituent materials, powders were dried overnight in a conventional oven. Different drying scenarios were followed between the pure PLA and nanocomposite materials. Pure PLA powder was dried for 24 h at 50 °C. PLA/MWCNTs nanocomposite materials were dried for 5 h at 50 °C. A suitable filament of 1.75 mm diameter was produced for every material concentration, using a 3D Evo (3D Evo B.V., Utrecht, the Netherlands) single screw extruder. The produced filament is going through quality control during the filament production procedure, with the real time diameter measurement system of the extruder.

Intamsys Funmat HT (Intamsys Technology ltd, Shanghai, China) 3D Printer was employed using an extruder's nozzle of 0.4 mm for the manufacturing of the specimens. [Figure 2](#) shows the 3D printing parameters used for the specimens' fabrication. All other parameters were set to their default values in

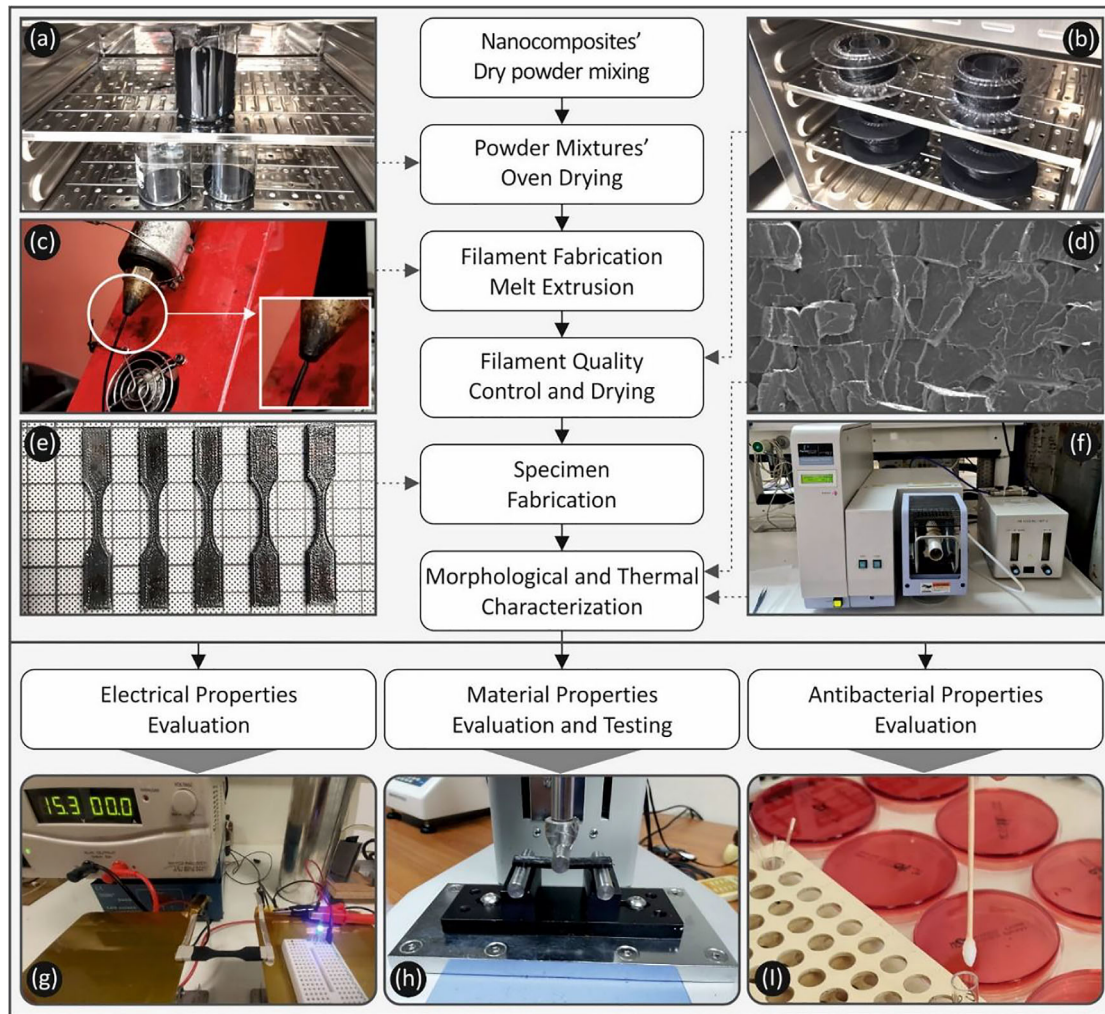


Figure 1. The methodology followed in this work to produce PLA/MWCNT nanocomposites and photos of the electrical/mechanical and antibacterial properties evaluation tests.

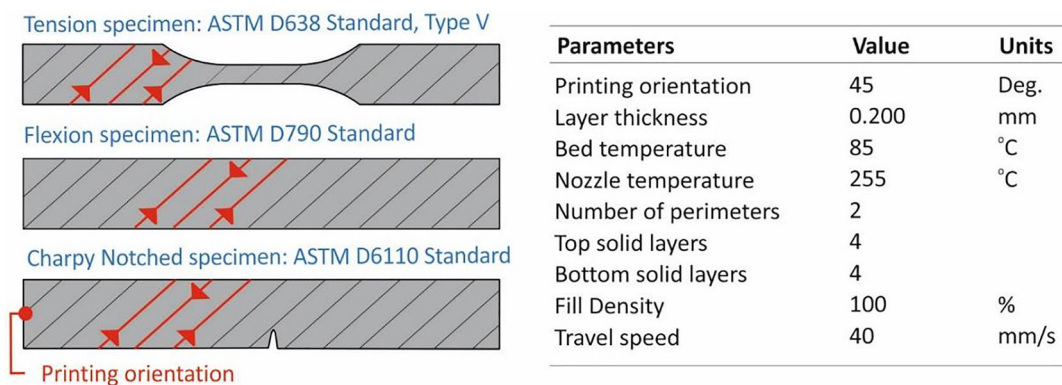


Figure 2. Settings used to fabricate the specimens in the 3D printer.

the Intamsuite software tool, which was used as the slicer software tool for this study.

2.3. Characterization techniques

American Society for Testing and Materials (ASTM) D638-02a international standard was followed in the tensile testing procedure. According to the standard, a type V specimen of 3.2 mm thickness was chosen, and five specimens were 3D printed and tested for

each case. Tensile tests were conducted on an Imada MX2 (Imada Inc., Northbrook, Illinois, United States) quasi-static testing apparatus, at a crosshead speed of 10 mm/min and room temperature conditions.

ASTM D790-10 (three-point bending test with 52.0 mm support span) international standard was followed in the flexural testing procedure. Tests were conducted at room temperature, with speed of 10 mm/min, on 64.0 mm length, 12.4 mm width, and

3.2 mm thickness specimens. Six specimens were tested for each material studied, on an Imada MX2 machine in flexural mode setup.

ASTM D6110-04 international standard was followed in the impact testing procedure. Notched specimens were tested in a Terco MT 220 (Terco, Kungens Kurva, Sweden) Charpy's impact apparatus. Release height of the apparatus hammer was the same for all the experiments (367 mm) and six specimens with the dimensions of 80.0 mm (length) \times 8.0 mm (width) \times 10.0 mm (thickness) were tested for each material prepared in this work.

Microhardness measurements were conducted according to the ASTM E384-17. The specimens' surface was fully polished before each set of measurements. An Innova Test 300-Vickers (Innovatest Europe BV, Maastricht, The Netherlands) apparatus was employed, while the applied force was set to 100 gF and duration of 10 s was selected for indentation. Imprints were measured under six different specimens for each one of the PLA and PLA/MWCNTS nanocomposites.

Dynamic Mechanical Analysis (DMA) was performed using a TA Instruments DMA850 instrument (New Castle, Delaware, United States). Samples were 3D printed in dimensions of length 58.0–60.0 mm, width 14.0–15.0 mm, and thickness 2.7–3.2 mm. Because of the samples having rough side edges from the FFF manufacturing process, all samples were polished in two steps using 240 and 400 grain sandpaper under water flow. Prior to testing, samples were dried at a temperature of 35 °C for 48 h minimum. DMA testing procedure consisted of a temperature ramp from room temperature to 130 °C (and in some cases up to 135 °C), at a rate of 3 °C min⁻¹. Testing was conducted using the three-point bending fixture. Samples were preloaded to 0.1 N. A sinusoidal displacement was applied to the samples with a constant amplitude of 30.0 μ m and a frequency of 1.0 Hz throughout the tests. Data were collected by the instrument at a sampling rate of 0.33 Hz. The recorded parameters were the storage modulus, loss modulus, temperature, time, tan δ , and oscillation angular frequency.

Scanning Electron Microscopy (SEM) characterization was used to analyze the nano/micro structuring of the 3D printed specimens' side surface, and the fractured surfaces of 3D printed tensile specimens. The SEM analysis was carried out using a JEOL JSM 6362LV (Jeol Ltd., Peabody, Massachusetts, United States) electron microscope in high-vacuum mode at 20 kV acceleration voltage on gold sputtered specimens.

The through-thickness (through-layer) as well as in-plane (cross-layer) electrical conductivity of 3D printed PLA/MWCNT nanocomposite samples was determined using square-shaped samples of 10.0 \times 10.0 mm² and 3.2 mm thickness. Ag paste

(room temperature fast curing curing/drying silver paste received from Agar Scientific Ltd, Essex, United Kingdom) was applied in the appropriate surfaces to contact the samples for the respective through-layer and cross-layer conductivity measurements. Afterwards, 2-point probe electrical resistance measurements were performed with an Agilent Multimeter (Agilent 34401A6^{1/2}, Agilent, Santa Clara, United States) to derive the electrical resistivity (ρ) and conductivity (σ), respectively, considering the specific sample dimensions.

Thermogravimetric analysis (TGA) was carried out for neat PLA, as well as the PLA/MWCNTs nanocomposites in nitrous (N₂) gas atmosphere, under a flow of 200 ml/min, with a Perkin Elmer Diamond TG/TDA (PerkinElmer, Inc., Waltham, Massachusetts, United States) device with a heating cycle from 40 °C to 550 °C and a heating step of 10 °C/min.

Raman spectroscopy was performed for the pure PLA, MWCNTs, and the PLA/MWCNT nanocomposite 3D printed specimens [48], using a Labram HR-Horiba (Kyoto, Japan) using a 514.5 nm line of an Ar⁺ ion laser. The laser power was set to 1.5 mW for all measurements at the focal plane to obtain the corresponding Raman spectra. For delivering the excitation light as well as collecting the back-scattering Raman activity, an optical microscope equipped with a 50 \times long working distance objective lens was used.

Antibacterial performance of the nanocomposites studied in this work, was investigated with the agar well diffusion method [49], carried out in a microbiological lab, for two different bacteria, *E. coli* and *S. aureus*. Petri dishes (85 mm in diameter) with suitable for each bacterium growth material (MC.2, C.010066 for the *E. coli* and Chapman, C.010068 for the *S. aureus*), were employed. Two rectangular specimens of 12.4 mm \times 12.4 mm and 3.2 mm height were 3D printed from pure PLA and the nanocomposite materials. The bacteria with the specimens were placed in an oven at 37 °C for 24 h for the diffusion of the antimicrobial agent into the nanocomposite and inhibit germination and growth of the test microorganism and the developed Inhibition Zone (IZ) was measured afterwards.

3. Results and discussion

3.1. Mechanical properties

3.1.1. Tensile test results

Figure 3 depicts the tensile properties [50] of each nanocomposite tested. Figure 3(a) shows tensile stress (MPa) to calculated Strain (mm/mm) graphs of a typical specimen tested of each sample. In Figure 3(b), the average tensile strength at break (MPa) for each material studied is shown to filler

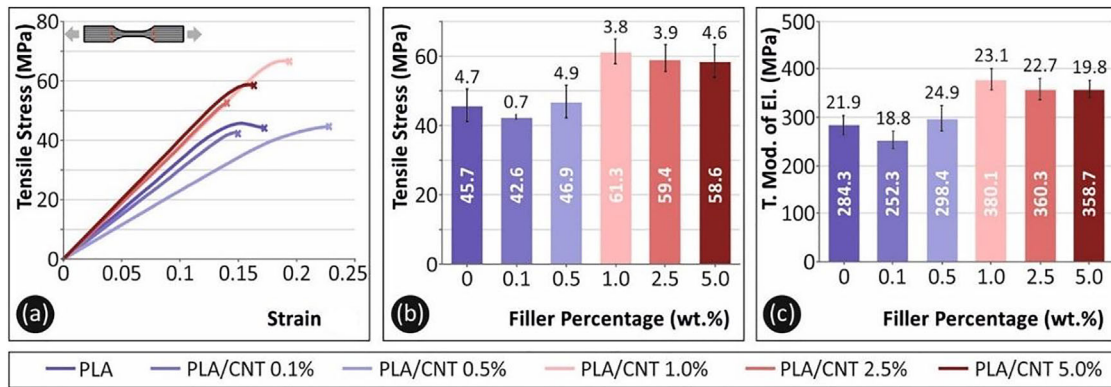


Figure 3. (a) Tensile Stress (MPa) vs. Strain (mm/mm) graph, for a characteristic specimen of each material. (b) Average maximum calculated Tensile Stress (at break) (MPa) to material's filler percentage (wt.%) graph. (c) Average Tensile Modulus of Elasticity (MPa) vs. Filler Percentage (wt.%) for each material fabricated.

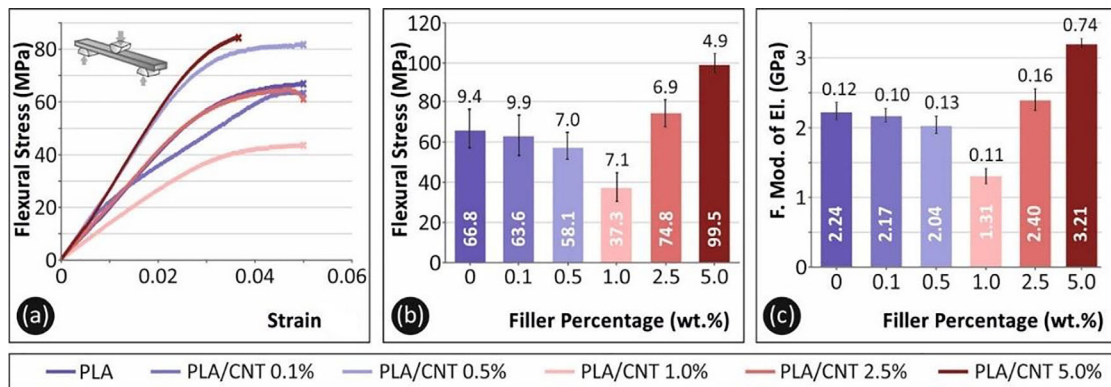


Figure 4. (a) Flexural Stress (MPa) vs. Strain (mm/mm) graph, for a characteristic specimen of each material. (b) Average maximum measured Tensile Stress (at break) (MPa) to each material's specimen Filler Percentage (wt.%) graph. (c) Average Tensile Modulus of Elasticity (MPa) vs. Filler Percentage (wt.%) for each material fabricated.

percentage (wt.%). The calculated average tensile modulus of elasticity (MPa) to filler percentage of each material tested is presented in Figure 3(c).

As shown in Figure 3, the MWCNTs do not significantly affect the tensile strength and modulus values up to 1.0 wt.% filler loading, while for loadings of 1 wt.% and higher the tensile properties are improved, compared to neat PLA. It should be mentioned that the tensile loading direction is 45° off-axis to the sample's printing direction, and therefore properties dominated and significantly affected by the adhesion between filaments. Specifically, an increase of both the tensile strength and the elastic modulus at 1.0, 2.5 and 5.0 wt.% filler loading could be observed. Namely, ~34% increase for the tensile strength and ~33% increase for the modulus of elasticity are the highest achieved improvements at 1.0 wt.% filler loading, while both at 2.5 and 5.0 wt.%, the tensile properties do not show any further improvement (revealing that at 1.0 wt.%, we have already achieved the mechanical percolation threshold for the tensile stress field). The slight decrease of the tensile properties at 2.5 and 5.0 wt.%, might be caused due to the hampering of the filamentous interfacial strength between adjacent filaments in the bulk 3D printed sample and/or limited interdiffusion of the polymeric chains from one

filament to another by the presence of MWCNTs fillers that could prevent extended polymer chain mobility in the melt state.

3.1.2. Flexural results

In Figure 4 the flexural properties [51] of each nanocomposite tested are presented. Figure 4(a) shows representative Flexural Stress (MPa) to Strain (mm/mm) curves for each material tested. Figure 4(b) shows the average Flexural Stress (MPa) to material's filler percentage (wt. %). Figure 4(c) shows the specimens' average calculated Flexural Modulus of Elasticity to the concentration of the filler for each material fabricated (wt.%). Regarding the flexural test results, the nanocomposites with 0.1 wt.%, 0.5 wt.% and 1.0 wt.% MWCNTs concentration showed a slight knock down effect when compared to pure PLA specimens. The highest flexural stress was measured at samples with 2.5 wt.% MWCNTs loading and 5.0 wt.%, representing an increase of ~12% for the flexural strength and ~7% for the flexural modulus for 2.5 wt.%, while for the 5.0 wt.% filler loading, the flexural strength increased ~49% and the flexural modulus ~43%. Overall, the introduction of MWCNT nanoparticles renders the PLA matrix more brittle. A plausible explanation behind this could be that CNTs are acting in general as nucleating agents and could

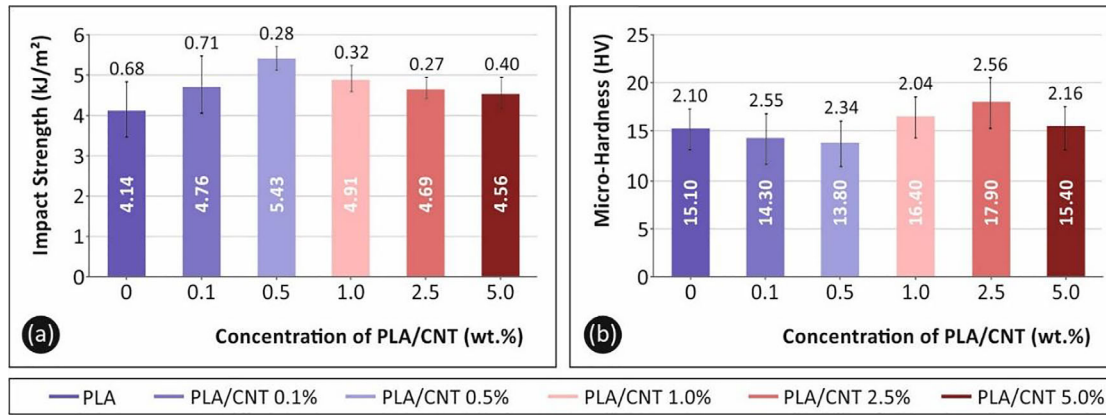


Figure 5. Impact and Microhardness properties of the fabricated materials (a) Charpy's notched impact test results (kJ/m^2). (b) Vickers Microhardness (HV) calculated for each nanocomposite concentration fabricated (wt.%).

increase thus the crystallinity of PLA, reflected to the increased modulus values, as have been similarly reported in previous studies [52].

3.1.3. Impact and microhardness results

Figure 5 illustrates the impact and micro-hardness properties of 3D printed PLA/MWCNTs nanocomposites and pure PLA. Figure 4(a) shows the average values of the Charpy's notched impact strength (kJ/m^2) results for each filler concentration. Figure 4(b) shows the average Vickers microhardness (HV) to material's filler percentage (wt.%). Regarding the average impact strength values (Figure 5a), in all filler loadings the impact strength is increasing. The highest increase of the impact strength was found in the 0.5 wt. % nanocomposite ($\sim 31\%$). The increasing of the micro-hardness is associated with the stiffening of the material induced by the MWCNTs nanocomposites in the PLA polymer matrix. Micro-hardness slightly decreases for the 0.1 and 0.5 wt.% nanocomposites, while it slightly increases for the 1.0 and 2.5 wt.%, with a slight decrease finally at the highest filled PLA at 5.0 wt.%. The most improved micro-hardness performance (Figure 5b) was observed for the 2.5 wt.% ($\sim 19\%$) nanocomposite.

3.2. Thermomechanical analysis

Figure 6 shows the 3D printed specimens' thermo-mechanical response, the storage modulus (MPa), loss modulus (MPa) and $\text{Tan } \delta$, as a function of temperature, derived from the DMA thermomechanical experiments, for the different filler loadings studied in this work. The values of storage modulus at low temperatures ($\sim 30^\circ\text{C}$) coincide with the flexural modulus of the 2.5 wt.% nanocomposite. The nature of the DMA set-up conditions and the samples' significantly lower dimensions are the reason of this samples' behavior. The increase in the storage moduli for the 2.5 wt.%, found by the DMA experiments ($\sim 12.5\%$) is associated with the reduced

mobility of the polymeric chains in the presence of MWCNT nanofillers.

As the temperature is increased, the storage modulus values drop. The $\text{Tan } \delta$ values for all samples tested show an increasing trend up to the temperature range of 55°C to 63°C , signifying that up to this temperature for each material, the mechanical energy is stored elastically in the polymeric macromolecular chains. On the other hand, $\text{Tan } \delta$ values drop for temperatures above the range of 61°C to 63°C revealing the softening of the material before fusion, and the transition to the viscoelastic regime.

3.3. SEM microstructural analysis

Figure 7 shows the side surface at $30\times$ and $150\times$ magnifications, while Figure 8 depicts the fractured area of tensile test specimens at $30\times$ and $1000\times$ magnifications, to illustrate the 3D printed specimens' microstructure characteristics. The 3D printed sample's microstructure, investigated from the side surface (Figure 7), could reveal the quality of 3D printing, showing the sample layers interface characteristics and interlayer fusion. This could lead to 3D nanocomposite parts with high mechanical performance, due to the presence of these specific nanofillers. The high-quality interlayer fusion proves that in this work the optimum 3D printing parameters were used to manufacture all the specimens and plausibly MWCNT nanofillers were homogeneously dispersed in the PLA produced filaments. Nanofiller's aggregations in the utilized filament could significantly affect the 3D printing quality by introducing inhomogeneities, discontinuities, etc. Such phenomena were not observed in this work.

Micrographs of the fractured area (Figure 8) reveal some discontinuities in the specimen's internal structure which become worst with the increase of the nanofillers' concentration. Such phenomena could be attributed to the failure effect during testing on the 3D printing structures. Overall,

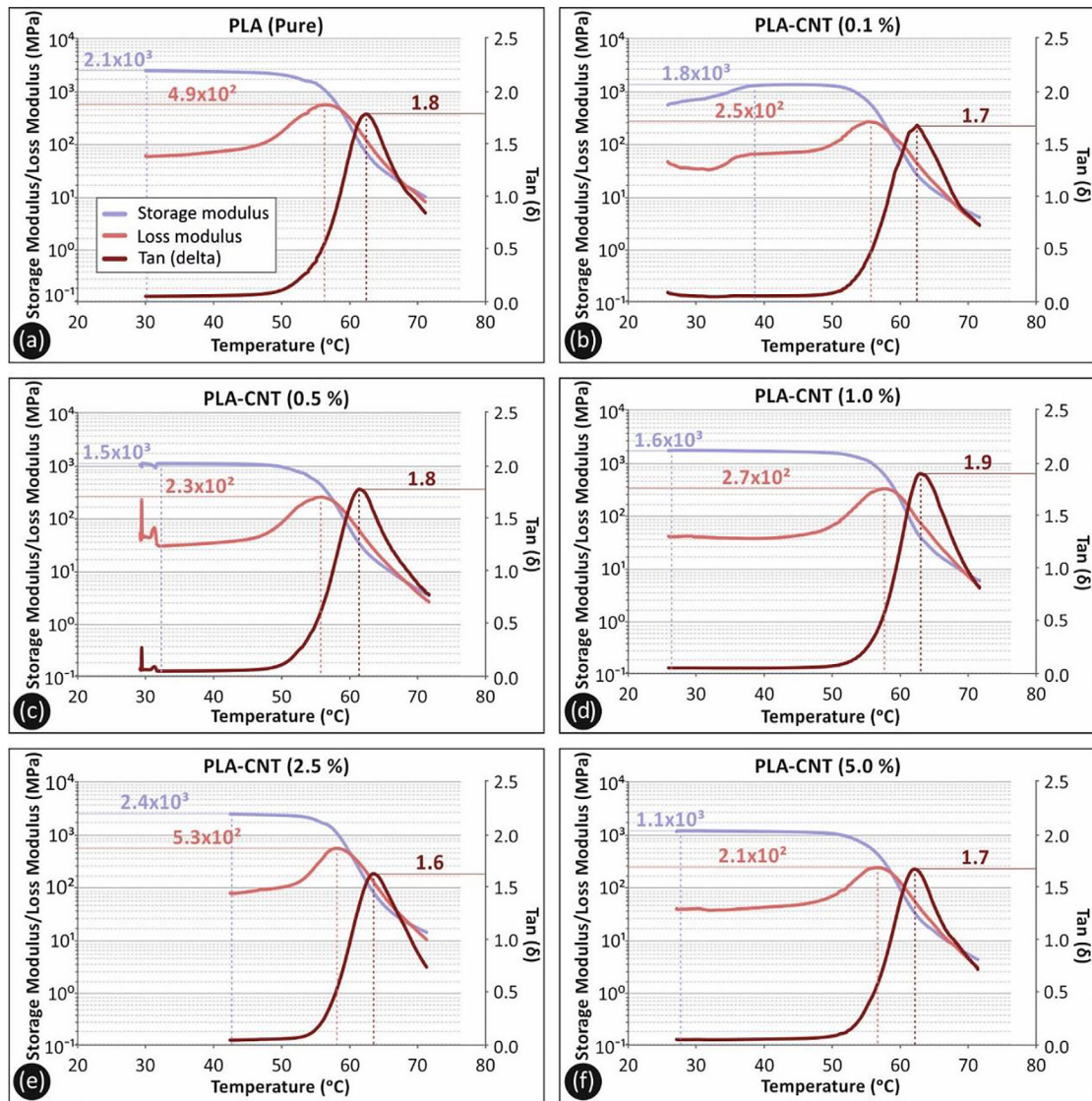


Figure 6. Storage modulus, loss modulus (MPa) and Tan(δ) plots of pure PLA and PLA/MWCNTs.

the fracture surfaces reveal a rather brittle failure of the filament strands.

3.4. Electrical conductivity

Figure 9 shows the procedure followed to determine the electrical conductivity of the 3D printed PLA/MWCNT nanocomposites. Figure 9(a) shows schematically the 2-probe electrical resistance to evaluate the electrical conductivity of the nanocomposites. In order to examine any anisotropic electrical conductivity behavior, which is significant in additive manufacturing produced specimens' behavior [53], the electrical conductivity has been measured in two different directions; one in the filamentous printing plane however off-axis of the 3D printed filaments (defined as 'cross-layer'; specifically off-axis at 45 degrees compared to the 45 degrees printing direction of the 3D printed samples), and one out-of-plane; perpendicular to the 3D printing direction and through the thickness of the 3D printed samples

(defined as 'through-layer' of the printed samples). Figure 9(b) shows the electrical conductivity of the PLA/MWCNTs nanocomposites at 1.0, 2.5 and 5.0 wt.% MWCNTs' concentrations in the nanocomposites. 'Through layer' and 'cross layer' are the two different measurement directions of the electrical conductivity implemented in this work. Figure 9(c) represents the electrical conductivity percolation curve for the 3D printed PLA/MWCNTs nanocomposites at different MWCNTs' concentrations, while as it can be observed the higher the CNT conductive filler loading, the higher the electrical conductivity achieved (in both directions), being in good agreement with previous studies about graphene nanoplatelet (GNP) 3D printed conductive nanocomposites [54].

Figure 9(d) shows the joule heating electrothermal performance of the highest electrically conductive PLA/MWCNTs nanocomposite sample (5.0 wt.%). The operation of a LED device when current is passing through a 5.0 wt.% filler loading

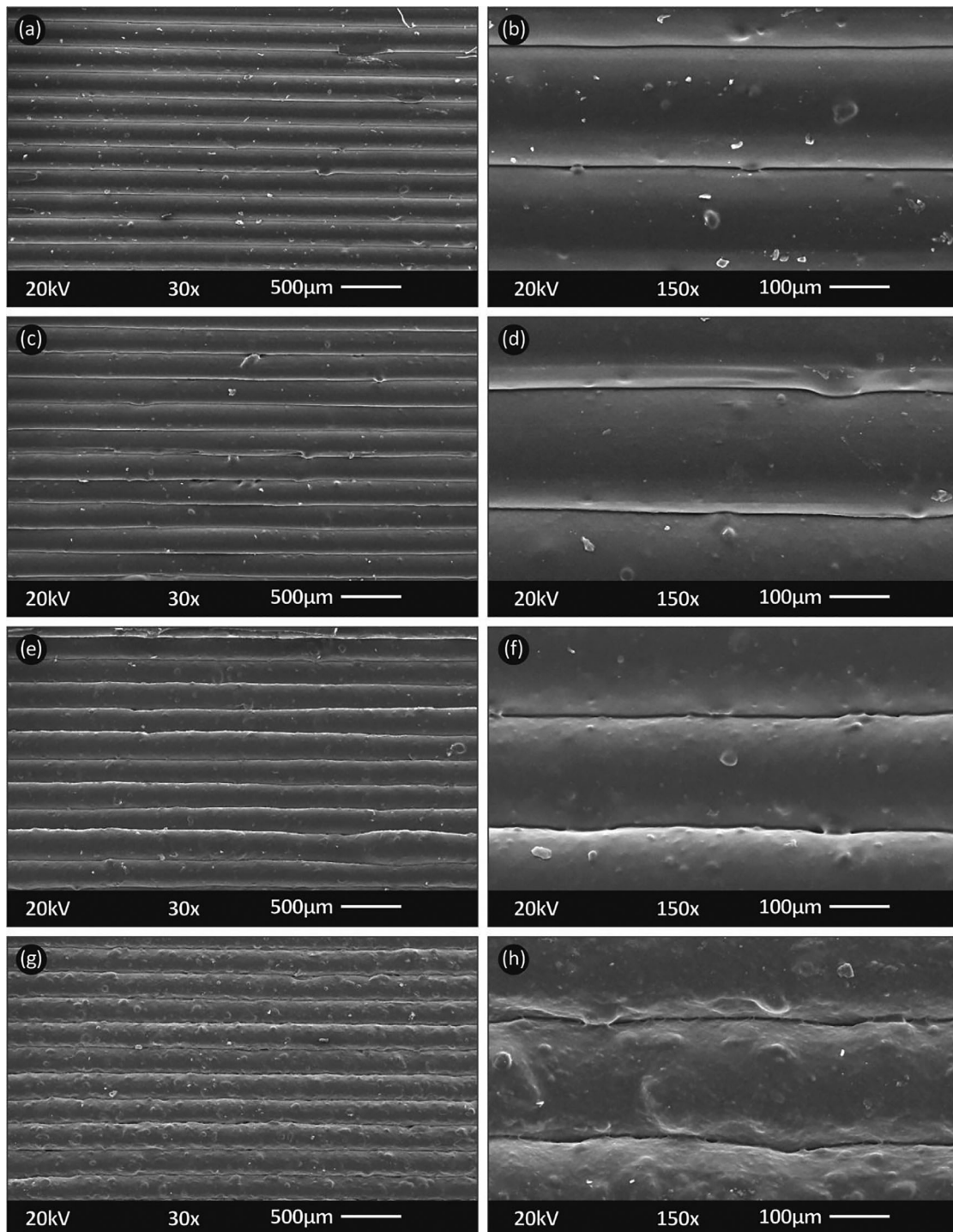


Figure 7. SEM images of the side surface for different filler loadings at two different magnifications: (a, b) PLA/MWCNTs 1.0 wt.%, (c, d) PLA/MWCNTs 2.5 wt.%, (e, f) PLA/MWCNTs 5.0 wt.%.

(more electrically conductive nanocomposite sample) in a closed circuit when a voltage bias (V_{bias}) of 15 V is applied is presented in Figure 9(e).

It is interesting to mention that for all 3D printed nanocomposites at different MWCNT contents, the ‘cross-layer’ conductivity values were a bit higher than the ‘through-layer’ ones, most likely attributed to the nature of the FFF 3D printing process endowing an ‘anisotropic’ character to the electrical properties of the final nanocomposites. More precisely, a plausible explanation for the slightly higher

electrical conductivity in the cross layer direction could be that (i) the 3D printing process induces some extent of CNT orientation in the print deposition direction, resulting thus in a slightly better ‘bulk’ electrical conductivity, as reported elsewhere for 3D printed CPCs [55], and (ii) the existence of some slight inhomogeneities, not perfect contact of the filaments at the different layers in the ‘through-layer’ direction, which might result in some evolution of slight contact resistance (this is not the case for the ‘cross-layer’ deposited/3D printed filaments).

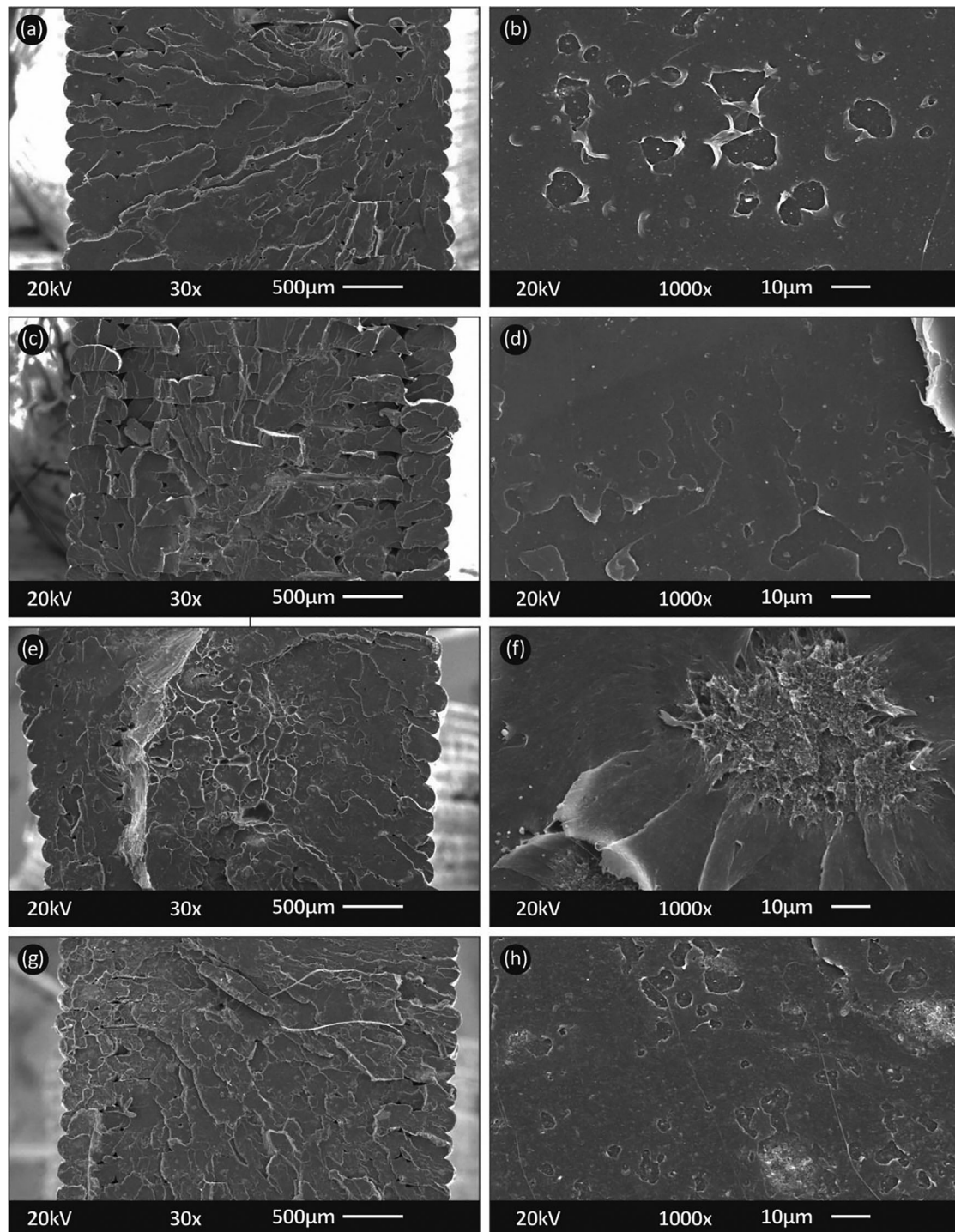


Figure 8. SEM images of the fracture area of tensile test specimens for different filler loadings at two different magnifications: (a, b) PLA/MWCNTs 0.5 wt.%, (c, d) PLA/MWCNTs 1.0 wt.%, (e, f), PLA/MWCNTs 2.5 wt.%, (g, h) PLA/MWCNTs 5.0 wt.%.

Regarding [Figure 9\(b\)](#), it can be observed that for all 3D printed PLA/MWCNTs nanocomposites, the cross-layer conductivity values are higher than the through thickness values. This is a proof that all the 3D printed nanocomposite samples exhibit anisotropic electrical transport properties induced by the FFF process. The highest conductivities were determined for the 5.0 wt.% PLA/MWCNTs nanocomposites. The small difference in the electrical conductivity values at the ‘through layer’ and ‘cross-layer’ directions, is a proof for the electrical

conductivity behaviour of the manufactured nanocomposites.

3.5. Thermogravimetric analysis (TGA)

[Figure 10](#) depicts the TGA ([Figure 9a](#)), and the DTG ([Figure 9b](#)) graphs of the 3D printed pure PLA, and PLA/MWCNTs nanocomposites. In the TGA graph three thermal windows can be observed. [Figure 10](#) shows that PLA/MWCNTs nanocomposite materials are thermally stable up to almost 270 °C

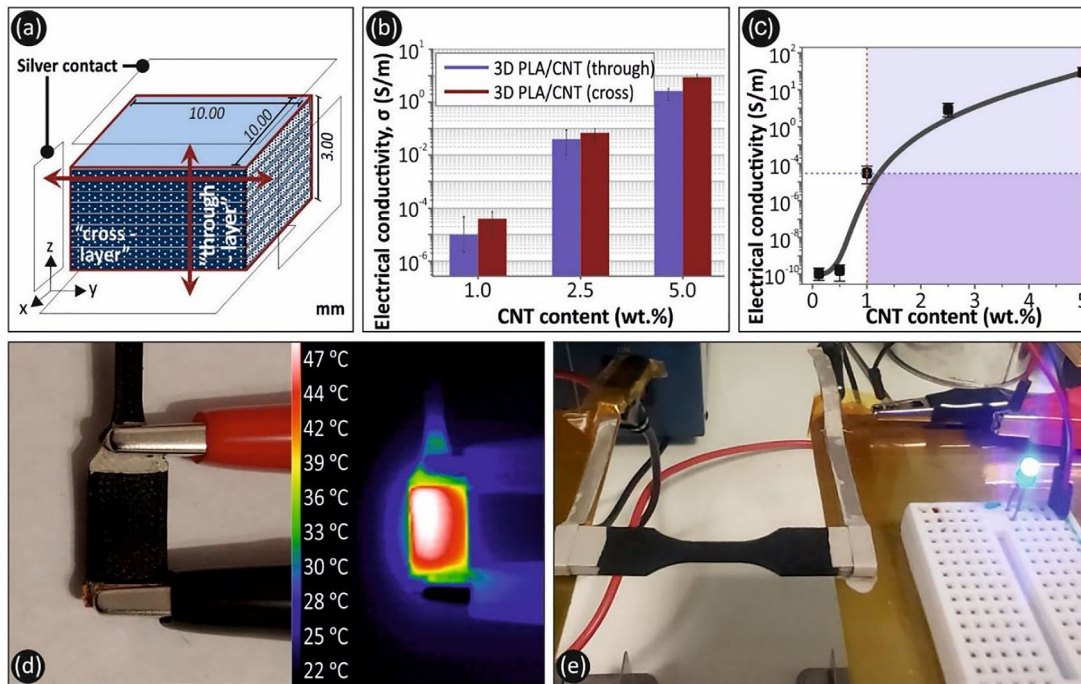


Figure 9. (a) Schematic diagram of the electrical conductivity measurements for the nanocomposites' specimens at two different directions. (b) Electrical conductivity of the 3D printed conductive nanocomposites at 1.0 wt.%, 2.5 wt.% and 5.0 wt.% filler loadings at two different measurement directions. (c) Electrical conductivity percolation curve for 3D printed PLA/MWCNTs 0.1 wt.%, 0.5 wt.%, 1.0 wt.%, 2.5 wt.% and 5.0 wt.% MWCNTs filler content. (d) A real sample digital image (left), and an IR-T image showing the electrothermal joule heating performance of the PLA/MWCNTs (5.0 wt.%) nanocomposite at an applied DC $V_{\text{bias}}=15\text{V}$ (right). (e) LED in operation in a closed circuit, when current is passing through PLA/MWCNTs (5.0 wt.%) nanocomposite with voltage bias $V_{\text{bias}} = 15\text{V}$ applied.

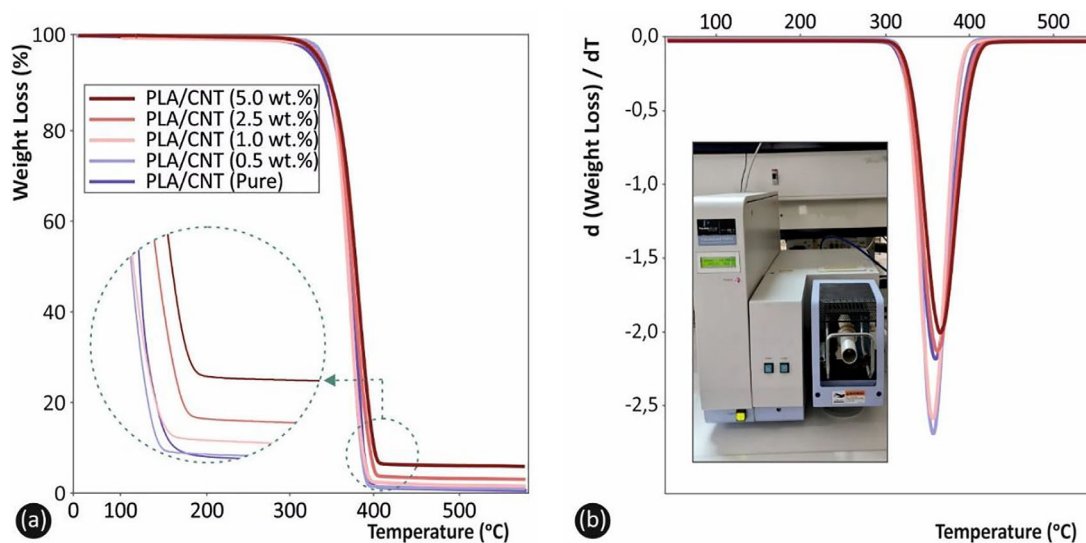


Figure 10. (a) Thermogravimetric analysis (TGA) and (b) differential thermogravimetry (DTG) plots of 3D printed neat PLA and PLA/MWCNTs nanocomposites at (0.5, 1.0, 2.5 and 5.0) wt.% filler loadings.

without any observed weight loss (%), this is the first temperature window. From 270 °C up to 390 °C, there is a second temperature window, corresponding to the materials' thermal degradation and decomposition with the onset temperature of decomposition (T_{on}) at 273 °C. In the third temperature window (>390 °C up to 550 °C), all the PLA substance for all samples' formulation has been fully decomposed.

3.6. Raman analysis

Figure 11 shows the Raman spectra of pure PLA, MWCNTs and the PLA/MWCNT nanocomposite at 2.5 wt.% filler loading. PLA presents a typical polymer Raman spectrum. On the other hand, PLA/MWCNTs (2.5 wt.% filler loading) nanocomposites, show totally different Raman fingerprints compares to the pure PLA. The unique D band at

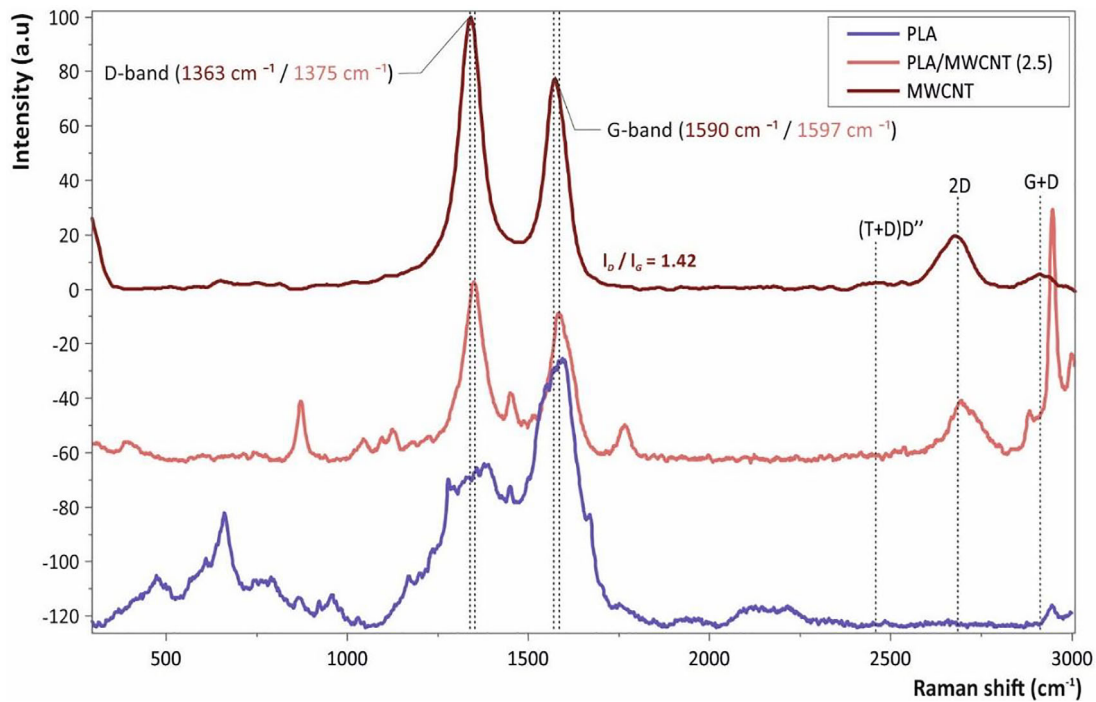


Figure 11. Raman spectra of pure PLA, MWCNTs and PLA/MWCNT nanocomposite at 2.5 wt.% filler percentage.

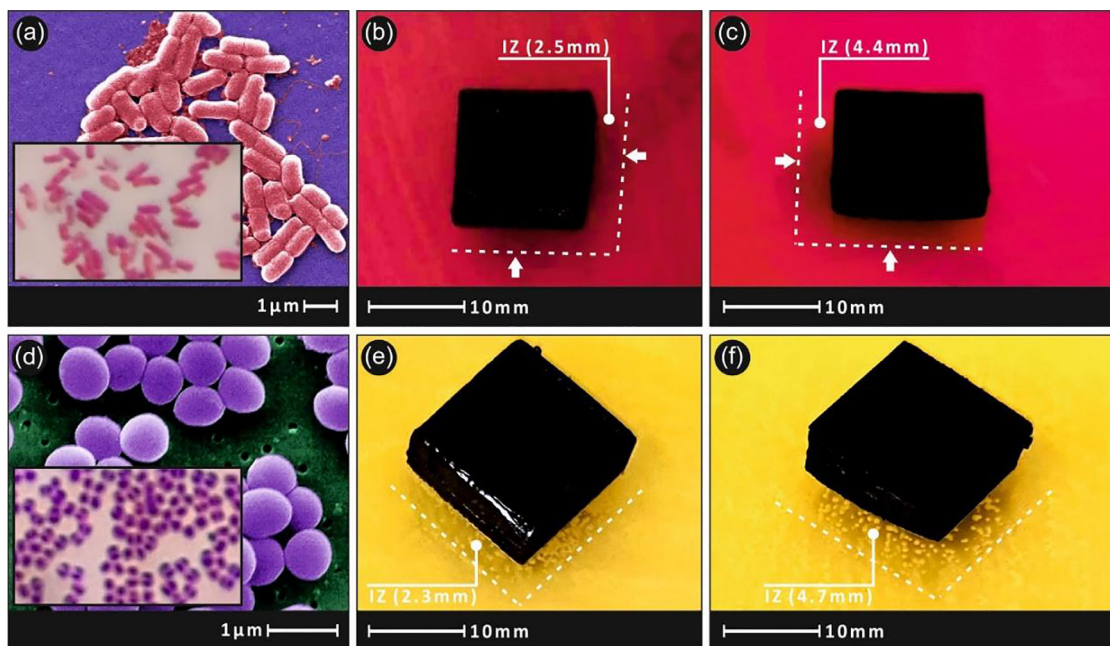


Figure 12. Pictures after the agar well diffusion method 24 h culture, showing the Inhibition Zone (IZ) of (a) *E. coli* against PLA/MWCNT (5.0 wt.%) (b–d) *S. aureus* against PLA/MWCNT (5.0 wt.%) (e, f).

$\sim 1330\text{ cm}^{-1}$ due to disorder-induced sp^3 hybridized carbon, and G band at $\sim 1582\text{ cm}^{-1}$ due to Raman spectrum, allowed tangential sp^2 hybridized carbons to be observed for the PLA/MWCNTs samples, confirming the existence of MWCNTs in the 3D printed materials. According to literature, intense G band relates to better nanotube dispersion in the polymer matrix [56], in this study the G band is very intensive indicating good dispersion of MWCNTs and corroborating the results by the SEM morphological analyses.

3.7. Antibacterial properties

Figure 12 presents the antibacterial results after the 24 h bacteria culture of the 5.0 wt.% concentration PLA/MWCNTs nanocomposite. The addition of MWCNTs in the PLA matrix material can introduce antibacterial properties to the polymer at least for the two bacteria tested in this study. The developed Inhibition Zone (IZ) was almost the same for both bacteria tested (*Staphylococcus aureus* and *Escherichia Coli*). The developed nanocomposite was 3D printed, so it is possible

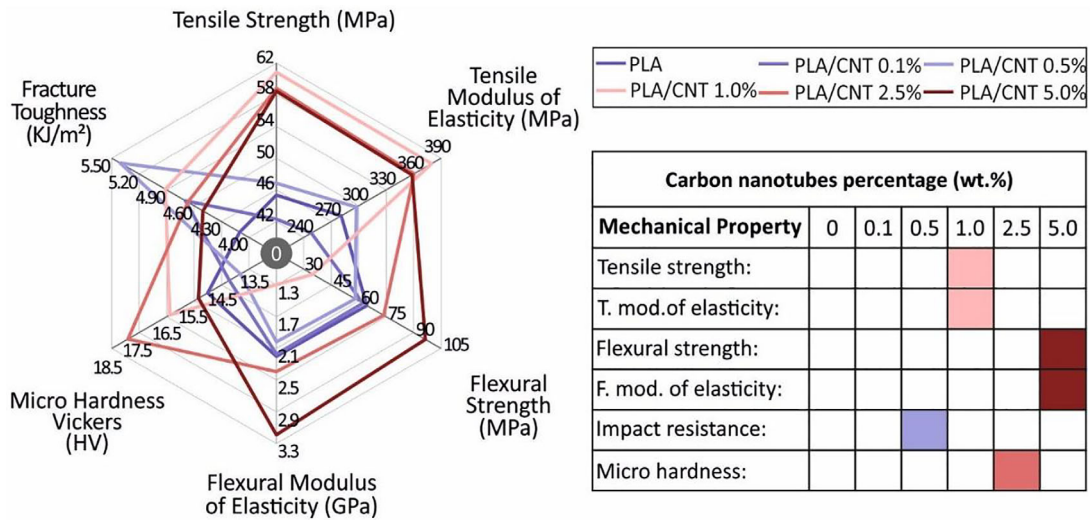


Figure 13. Summary of the mechanical properties results for all materials tested in this study.

to be employed in building parts for biomedical applications.

4. Conclusions

PLA/MWCNTs nanocomposites at 0.5, 1.0, 2.5 and 5.0 wt.% filler loadings were prepared; a melt mixing method followed by a filament extrusion process were implemented, to produce novel multifunctional materials for application in the FFF 3D printing technology. Figure 13 summarizes the mechanical properties determined in the study for all the samples printed at 45 degrees).

The addition of MWCNTs in the PLA matrix improved the mechanical properties and rendered the nanocomposites electrically conductive, while a mild antibacterial performance was determined for the higher filler loading tested in this work. Such materials can be employed in industrial applications requiring enhanced properties in multiple fields, such as in sensors, medicine, etc.

It is believed that the best reinforcing mechanism should theoretically arise from the 5.0 wt.% filler loading for all the different mechanical properties reported. However, this is the case only for the flexural properties investigated in our study, and especially not for the tensile, Impact and Microhardness properties that a knock-down effect has been observed for filler loadings >1.0 wt.%. This could be more precisely attributed to the fact that at 5.0 wt.%, already some aggregates of CNTs might appear in the PLA matrix, which negatively affect the tensile, Impact and Microhardness properties. Moreover, the strain field generated during the flexural experiments i.e. combined bending and tension strain fields, in conjunction with the 3D printed nature/structure of the samples is not getting affected by the presence of these plausible microstructural

defects (CNT aggregates), resulting into an experimentally obtained enhancement in flexural modulus and strength of the resulting PLA/CNT 3D printed nanocomposites.

As a future work, a significant challenge might be to investigate thoroughly and enhance the dispersion and/or possible some alignment of MWCNTs in the PLA matrix during the FFF filamentous extrusion based process, since MWCNTs tend to agglomerate due to Van der Waals forces and it is extremely difficult to disperse them in the polymer melt (especially for loadings above 1.0 wt.% as it might be also the case of our study).

Acknowledgments

Authors would like to thank Ms Aleka Manousaki from the Institute of Electronic Structure and Laser of the Foundation for Research and Technology-Hellas (IESL-FORTH) for taking the SEM images presented in this work.

Disclosure statement

The authors declare no conflict of interest. The funding sponsors had no role in the design of the study; in the collection, analyses, or interpretation of data; in the writing of the manuscript, and in the decision to publish the results. Journal policies have been reviewed and accepted by all authors.

ORCID

Markos Petousis  <http://orcid.org/0000-0003-1312-7898>

Data availability statement

The raw/processed data required to reproduce these findings cannot be shared at this time due to technical or time limitations.

Submission declaration and verification

The work has not been published previously and it is not under consideration for publication elsewhere. Its publication is approved by all authors and tacitly or explicitly by the responsible authorities where the work was carried out, and, if accepted, it will not be published elsewhere in the same form, in English or in any other language, including electronically without the written consent of the copyright-holder.

Notes on contributors

Dr. Nectarios Vidakis is a Professor of the Mechanical Engineering Department of Hellenic Mediterranean University the Head (Lab Director) of the Laboratory for Precision Machining, Reverse Engineering and Biomechanics (PMREB Lab). The laboratory (among others) has equipment and experience for CNC machining processes, 3d printing, 3d scanning and vacuum casting processes. His academic and research interests include: Industrial and Production Technologies, Numerical Control, CAD/CAM/CAE Systems, Industrial Design Optimization, Reverse Engineering, Rapid Prototyping, Materials Testing and Characterization, Nano-materials and Composites, as well as biomechanics.

Markos Petousis is a Dr. Mechanical Engineer. His Phd is in the area of virtual reality and machining processes simulation. Currently, he is an Assistant Professor at the Mechanical Engineering Department of the Hellenic Mediterranean University, where he teaches CAD/CAM/CNC, 3D printing and machining processes. His main research interests are three-dimensional geometric modeling, computer graphics, biomechanics, physical and virtual mockups development, additive manufacturing, Polymers and nanomaterials in 3D printing, reverse engineering and prototyping techniques. So far, he has fifty journal publications, forty-three international scientific conferences publications and three book chapters. In the past he has worked in several successfully completed research projects funded by European and National resources.

Mirto Kourinou received her B.Sc. in physics from the University of Crete in 2017, and her M.Sc. in Microsystems and Nanodevices from the National Technical University of Athens in 2019. Now she is currently Ph.D. student in the Laboratory of Precision Manufacturing and Reverse Engineering, Mechanical Engineering Department, Hellenic Mediterranean University. Her research focusing on 3D printed nanomaterials and their biomedical applications.

Mr Emmanuel Velidakis received his MSc Diploma in Mechanical Engineering from National Technical University of Athens in 2012. From 2012 until 2016 he served as a Service Manager and as Production Assistant Manager in two (2) different industries in Greece. Since 2016 he works in his own company, specialized in Additive Manufacturing and Reverse Engineering. From 2019 he is a PhD Candidate in Hellenic Mediterranean University with interest in material science of Fused Filament Fabrication AM technique.

Nikolaos Mountakis received the B.Sc in Mechanical Engineering from Technological Educational Institute of Crete in 2017, currently studying MSc in Advanced

Manufacturing Systems, Automation and Robotics. Is a research assistant at the Precision Machining, Reverse Engineering and Biomechanics laboratory of Hellenic Mediterranean University of Crete. His current research interest focuses on nanomaterials fabrication for additive manufacturing technologies and CAD/CAM systems.

Peder Erik Fischer-Griffiths is a PhD candidate at the Department of Manufacturing and Civil Engineering of the Norwegian University of Science and Technology, under the supervision of Prof. Sotirios Grammatikos. His main interests are related to materials engineering, polymer and nanomaterials. He is a Dynamic Mechanical Analysis expert.

Sotirios Grammatikos is a Professor in Polymers and Composites at the Dept. of Manufacturing and Civil Engineering, Scientific Director of the Advanced and Sustainable Engineered Materials Laboratory (asemlab.no) and Leader of the Research Group Sustainable Composites. Sotirios is also an Affiliated Professor at Chalmers University of Technology in Sweden, and Visiting Scientist at the Hellenic Mediterranean University in Greece. He is a Materials Engineer, specialized in the area of product development, characterization, assessment and structural health monitoring of advanced composite materials and structures in aerospace, renewable energy, automotive and civil engineering applications. His main research interests are smart features of polymer composites, cement and asphalt composites (i.e. self-sensing, energy harvesting, etc.) enabled by nanotechnology, natural (green) materials, recycling and durability aspects. Before joining NTNU, he was a Research Fellow at Chalmers University of Technology, Sweden (2016-2017) and previously a Research Associate at the University of Bath, UK (2014-2015) and a Post-doc at the University of Ioannina (2013). He holds a PhD in Materials Engineering specialized in Structural Integrity of Aerostructures (2009-2013), a MSc in Chemistry & Technology of Materials (2008-2010) and a diploma in Materials Science & Engineering from the University of Ioannina, Greece (2003-2008). He has received training in lightweight aerospace composites from the Hellenic Aerospace Industry (HAI), Athens, Greece (2008).

Dr. Lazaros Tzounis received a Diploma of Materials Science & Engineering, from the University of Ioannina, Greece in 2010. He moved then to Germany to conduct his PhD at the Technical University of Dresden, completed in 2014. He specialises in novel Thermoelectrics, Polymer Nanocomposites, Nanotechnology, Additive Manufacturing (AM) and Fiber reinforced Polymer Composites. Currently he is an Associate Professor at the Hellenic Mediterranean University, Greece at the Mechanical Engineering Department focusing on 2D and 3D printing. He is the author of >80 scientific publications with over 2,400 total citations.

References

1. Muhammed Shameem M, Sasikanth SM, Annamalai R, et al. A brief review on polymer nanocomposites and its applications. Mater Today: Proc. 2021;45: 2536–2539.
2. Kononova S, Gubanova G, Korytkova E, et al. Polymer nanocomposite membranes. Appl Sci. 2018;8(7):1181.

3. Hassan T, Salam A, Khan A, et al. Functional nanocomposites and their potential applications: a review. *J Polym Res*. 2021;28(2). <https://doi.org/10.1007/s10965-021-02408-1>.
4. Bocharov GS, Eletsii AV. Percolation conduction of carbon nanocomposites. *IJMS*. 2020;21(20):7634.
5. Czaniková K, Špitalský Z, Krupa I, et al. Electrical and mechanical properties of ethylene vinyl acetate based composites. *MSF*. 2012;714:193–199.
6. Liebscher M, Tzounis L, Junger D, et al. Electrical joule heating of cementitious nanocomposites filled with multi-walled carbon nanotubes: role of filler concentration, water content, and cement age. *Smart Mater Struct*. 2020;29(12):125019..
7. Doagou-Rad S, Islam A, Jensen JS. Influence of processing conditions on the mechanical behavior of MWCNT reinforced thermoplastic nanocomposites. *Procedia CIRP*. 2017;66:131–136.
8. Deng L, Eichhorn SJ, Kao C-C, et al. The effective Young's modulus of carbon nanotubes in composites. *ACS Appl Mater Interfaces*. 2011;3(2):433–440.
9. Raj A, Samuel C, Malladi N, et al. Enhanced (thermo)mechanical properties in biobased poly(l-lactide)/poly(amide-12) blends using high shear extrusion processing without compatibilizers. *Polym Eng Sci*. 2020;60(8):1902–1916.
10. García Ibarra V, Sendón R, Rodríguez-Bernaldo de Quirós A. 2016. Antimicrobial food packaging based on biodegradable materials. In *Antimicrobial food packaging*. Amsterdam, Netherlands: Elsevier. p. 363–384.
11. Vidakis N, Petousis M, Tzounis L, et al. Sustainable additive manufacturing: mechanical response of polyamide 12 over multiple recycling processes. *Materials*. 2021;14(2):466.
12. Tzounis L, Bangeas PI, Exadaktylos A, et al. Three-dimensional printed polylactic acid (PLA) surgical retractors with sonochemically immobilized silver nanoparticles: the next generation of low-cost antimicrobial surgery equipment. *Nanomaterials*. 2020;10(5):985.
13. Leal Filho W, Saari U, Fedoruk M, et al. An overview of the problems posed by plastic products and the role of extended producer responsibility in Europe. *J Cleaner Prod*. 2019;214:550–558.
14. Gonçalves de Moura I, Vasconcelos de Sá A, Lemos Machado Abreu AS, et al. 2017. Bioplastics from agro-wastes for food packaging applications. In *Food packaging*. Amsterdam, Netherlands: Elsevier. p. 223–263.
15. Zaaba NF, Jaafar M. A review on degradation mechanisms of polylactic acid: hydrolytic, photodegradative, microbial, and enzymatic degradation. *Polym Eng Sci*. 2020;60(9):2061–2075.
16. Lim L-T, Auras R, Rubino M. Processing technologies for poly(lactic acid). *Prog Polym Sci*. 2008;33(8):820–852.
17. Kumar N, Das D. Fibrous biocomposites from nettle (*girardinia diversifolia*) and poly(lactic acid) fibers for automotive dashboard panel application. *Compos B: Eng*. 2017;130:54–63.
18. Tanase CE, Spiridon I. PLA/chitosan/keratin composites for biomedical applications. *Mater Sci Eng C Mater Biol Appl*. 2014;40:242–247.
19. Devaux E, Aubry C, Campagne C, et al. PLA/carbon nanotubes multifilament yarns for relative humidity textile sensor. *J Eng Fibers Fabr*. 2011;6(3):155892501100600.
20. Ilyas RA, Sapuan SM, Harussani MM, et al. Polylactic acid (PLA) biocomposite: processing, additive manufacturing and advanced applications. *Polymers*. 2021;13(8):1326.
21. Vidakis N, Petousis M, Velidakis E, et al. Enhanced mechanical, thermal and antimicrobial properties of additively manufactured polylactic acid with optimized nano silica content. *Nanomaterials*. 2021;11(4):1012.
22. Bardot M, Schulz MD. Biodegradable poly(lactic acid) nanocomposites for fused deposition modeling 3D printing. *Nanomaterials*. 2020;10(12):2567.
23. Ford S, Despeisse M. Additive manufacturing and sustainability: an exploratory study of the advantages and challenges. *J Cleaner Prod*. 2016;137:1573–1587.
24. Vidakis N, Petousis M, Maniadi A, et al. Sustainable additive manufacturing: mechanical response of Acrylonitrile-Butadiene-Styrene over multiple recycling processes. *Sustainability*. 2020;12(9):3568.
25. Jouni M, Djurado D, Massardier V, et al. A representative and comprehensive review of the electrical and thermal properties of polymer composites with carbon nanotube and other nanoparticle fillers. *Polym Int*. 2017;66(9):1237–1251.
26. Ferreira I, Melo C, Neto R, et al. Study of the annealing influence on the mechanical performance of PA12 and PA12 fibre reinforced FFF printed specimens. *RPJ*. 2020;26(10):1761–1770.
27. Vidakis N, Petousis M, Vairis A, et al. On the compressive behavior of an FDM steward platform part. *J Comput Des Eng*. 2017;4(4):339–346.
28. Takagishi K, Umezu S. Development of the improving process for the 3D printed structure. *Sci Rep*. 2017;7(1):39852.
29. Vidakis N, Petousis M, Velidakis E, et al. On the strain rate sensitivity of fused filament fabrication (FFF) processed PLA, ABS, PETG, PA6, and PP thermoplastic polymers. *Polymers*. 2020;12(12):2924.
30. Vidakis N, Petousis M, Velidakis E, et al. Three-dimensional printed antimicrobial objects of polylactic acid (PLA)-silver nanoparticle nanocomposite filaments produced by an in-Situ reduction reactive melt mixing process. *Biomimetics*. 2020;5(3):42.
31. Sharma PC, Sharma D, Sharma A, et al. Hydrazone comprising compounds as promising anti-infective agents: chemistry and structure-property relationship. *Mater Today Chem*. 2020;18:100349.
32. Venkatesan J, Kim S-K, Shim M. Antimicrobial, antioxidant, and anticancer activities of biosynthesized silver nanoparticles using marine algae *ecklonia cava*. *Nanomaterials*. 2016;6(12):235.
33. Ahmed W, Zhai Z, Gao C. Adaptive antibacterial biomaterial surfaces and their applications. *Mater Today Bio*. 2019;2:100017.
34. Qiu H, Si Z, Luo Y, et al. The mechanisms and the applications of antibacterial polymers in surface modification on medical Devices. *Front Bioeng Biotechnol*. 2020;8:910.
35. Kamaruzzaman NF, Tan LP, Hamdan RH, et al. Antimicrobial polymers: the potential replacement of existing antibiotics? *IJMS*. 2019;20(11):2747.

36. Tzounis L, Zappalorto M, Panozzo F, et al. Highly conductive ultra-sensitive SWCNT-coated glass fiber reinforcements for laminate composites structural health monitoring. *Compos B: Eng.* **2019**;169:37–44.
37. Patanwala HS, Hong D, Vora SR, et al. The microstructure and mechanical properties of 3D printed carbon nanotube-poly(lactic acid) composites. *Polym Compos.* **2018**;39(S2):E1060–E1071.
38. Han T, Kundu S, Nag A, et al. 3D printed sensors for biomedical applications: a review. *Sensors.* **2019**;19(7):1706.
39. Christ JF, Aliheidari N, Ameli A, et al. 3D printed highly elastic strain sensors of multiwalled carbon nanotube/thermoplastic polyurethane nanocomposites. *Mater Des.* **2017**;131:394–401.
40. Haghiashtiani G, Habtour E, Park S-H, et al. 3D printed electrically-driven soft actuators. *Extreme Mech Lett.* **2018**;21:1–8.
41. Jaksic NI, Desai PD. Characterization of resistors created by fused filament fabrication using electrically-conductive filament. *Procedia Manuf.* **2018**;17:37–44.
42. Yang L, Li S, Zhou X, et al. Effects of carbon nanotube on the thermal, mechanical, and electrical properties of PLA/CNT printed parts in the FDM process. *Synth Met.* **2019**;253:122–130.
43. Mora A, Verma P, Kumar S. Electrical conductivity of CNT/polymer composites: 3D printing, measurements and modeling. *Compos B: Eng.* **2020**;183:107600.
44. Vidakis N, Petousis M, Velidakis E, Mountakis N, et al. Fused filament fabrication three-dimensional printing Multi-Functional of poly(lactic acid)/carbon black nanocomposites. *C.* **2021**;7(3):52.
45. Gnanasekaran K, Heijmans T, van Bennekom S, et al. 3D printing of CNT- and graphene-based conductive polymer nanocomposites by fused deposition modeling. *Appl Mater Today.* **2017**;9:21–28.
46. Aumnate C, Potiyaraj P, Saengow C, et al. Reinforcing polypropylene with graphene-poly(lactic acid) microcapsules for fused-filament fabrication. *Mater Des.* **2021**;198:109329.
47. Shmueli Y, Lin Y-C, Zuo X, et al. In-situ X-ray scattering study of isotactic polypropylene/graphene nanocomposites under shear during fused deposition modeling 3D printing. *Compos Sci Technol.* **2020**;196:108227.
48. Ferrari AC, Basko DM. Raman spectroscopy as a versatile tool for studying the properties of graphene. *Nat Nanotechnol.* **2013**;8(4):235–246.
49. Balouiri M, Sadiki M, Ibsouda SK. Methods for in vitro evaluating antimicrobial activity: a review. *J Pharm Anal.* **2016**;6(2):71–79.
50. Vidakis N, Petousis M, Tzounis L, et al. Polyamide 12/multiwalled carbon nanotube and carbon black nanocomposites manufactured by 3D printing fused filament fabrication: a comparison of the electrical, thermoelectric, and mechanical properties. *C.* **2021**;7(2):38.
51. Goh GD, Yap YL, Tan HKJ, et al. Process–structure–properties in polymer additive manufacturing via material extrusion: a review. *Crit Rev Solid State Mater Sci.* **2020**;45(2):113–133.
52. Murariu M, Dechief A-L, Ramy-Ratiarison R, et al. Recent advances in production of poly(lactic acid) (PLA) nanocomposites: a versatile method to tune crystallization properties of PLA. *Nanocomposites.* **2015**;1(2):71–82.
53. Somireddy M, Czekanski A. Anisotropic material behavior of 3D printed composite structures – material extrusion additive manufacturing. *Mater Des.* **2020**;195:108953.
54. Gao Y, Picot OT, Zhang H, et al. Synergistic effects of filler size on thermal annealing-induced percolation in poly(lactic acid) (PLA)/graphite nanoplatelet (GNP) nanocomposites. *Nanocomposites.* **2017**;3(2):67–75.
55. Sierra-Romero A, Chen B. Strategies for the preparation of polymer composites with complex alignment of the dispersed phase. *Nanocomposites.* **2018**;4(4):137–155.
56. Ivanov E, Kotsilkova R, Krusteva E. Effect of processing on rheological properties and structure development of EPOXY/MWCNT nanocomposites. *J Nanopart Res.* **2011**;13(8):3393–3403.